Atmospheric Ozone as A Climate Gas

Wei-Chyung Wang[1], Sun Wong[1], Jing Wang[1], Huiting Mao[1], Xin-Zhong Liang[1], and Ivar Isaksen[2]

(1) Atmospheric Sciences Research Center, State University of New York at Albany; (2) Geophysics Institute, University of Oslo, Norway. [February 23-25, 1999 ACP Science Team Meeting]

Project Objectives

To develop and apply climate-chemistry models for:

- Understanding the physical, chemical and dynamic processes that control mid-latitude O_3 in the lower stratosphere and free troposphere;
- Developing improved predictions of future O_3 changes in these regions and their influence on (and response to) future climate changes due to increasing greenhouse gases CO_2, N_2O, CH_4 and the CFCs, and changes of O_3 precursor gases.

Research Progress

- Seasonal-to-interannual variability of total ozone and tropopause [submitted to *J. Atmos. Sci*.]
- The effect of cirrus cloud on photodissociation rate coefficients $J(O^1D)$ and $J(NO_2)$ [in draft]
- The impact on radiative forcing from aircraft emissions
- The SUNYA-AMIP(II) ozone experiments

1. Seasonal-to-Interannual Variability of Total Ozone and Tropopause

Approximately 80% of total ozone is concentrated in the lower stratosphere where ozone variations are controlled by atmospheric motion. Consequently, strong interactions exist among total ozone, tropopause and dynamics on the seasonal-to-interannual time scales. In this study, we use the global TOMS measurements, outgoing longwave radiation (OLR) observations and NCEP/NCAR reanalysis data during 1979-1998 to construct a comprehensive dynamical picture of these interactions and the underlying mechanisms. To facilitate the study, we separate for each variable its interannual anomalies from the annual cycle and eddies from the zonal mean, and conduct diagnoses on individual and composite components to illustrate physically robust signals. Two regimes with distinctively different physical and dynamical characteristics are identified, as shown in Fig. 1.

In the tropics and subtropics, the annual cycle of zonal mean total ozone is dominated by the extratropical stratospheric wave-induced suction while its interannual variation follows the equatorial stratospheric quasi-biennial oscillation. The corresponding eddy patterns are created by baroclinic equatorial wave adjustment to the localized heating that results from climatological and El Niño-Southern Oscillation related convective activities. These processes induce vigorous lower stratospheric vertical motions, whose advection effect essentially determines total ozone variations. Therefore, the tropopause serves mainly as a transition zone, where considerable stratosphere-troposphere air mass exchange occurs. In the extratropics, three mechanisms are predominant in total ozone variations. The meridional transport associated with the Brewer-Dobson circulation governs the zonal-mean annual cycle. The extratropical and equatorial quasi-biennial oscillations exert, respectively, direct and indirect control on zonal-mean interannual anomalies during local winter and spring. The tropopause vertical displacement dominates the eddy structure throughout the year. In this regard, the tropopause acts primarily as a material surface, with which the lower stratospheric ozone-rich layer rises up and down.

The results indicate that the troposphere and stratosphere are strongly coupled through distinct dynamical processes across the tropopause. Such coupling must be explicitly treated in an interactive climate-chemistry model, which shall be validated against the physical mechanisms identified in this study.

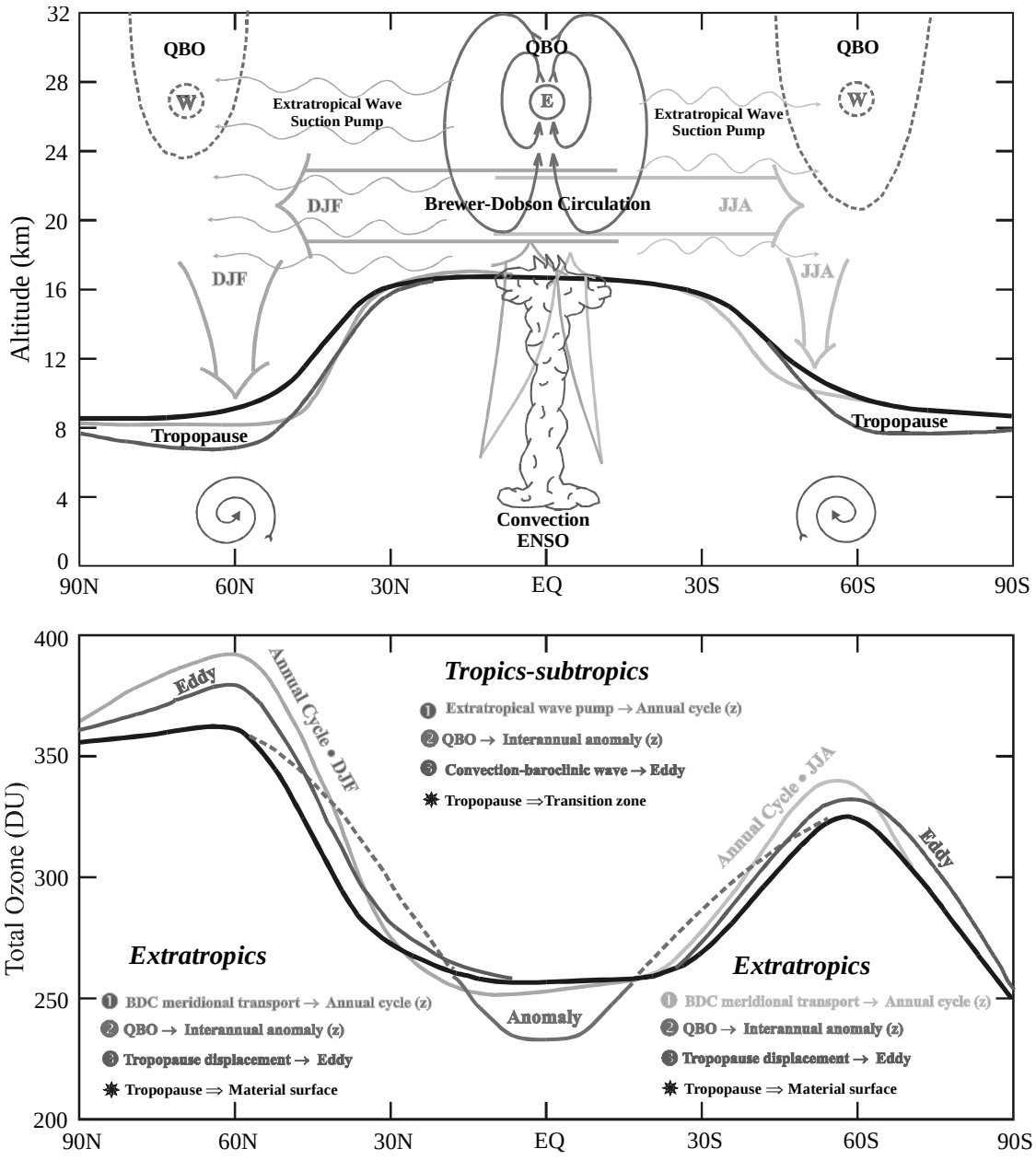

Fig. 1. A dynamical picture that depicts total ozone (*lower*) and tropopause (*upper*) seasonal-interannual variations, their associations and underlying mechanisms. Black curves illustrate the annual, zonal mean distribution. Green and orange curves show the DJF and JJA phases of the annual cycle. Blue curves describe QBO induced interannual anomalies. Red and pink curves delineate eddy responses that result from tropopause displacements and baroclinic wave adjustment to convective heating. Arrows denote for flow directions and wavy curves for wave activities. Circled W and E represent the polar night stratospheric westerly jet and the QBO easterly phase. Solid curves indicate features that are active throughout the year, while dashed ones identify signals, which operate only during local winter and spring (weaker).

2. The Effect of Cirrus Clouds on Photodissociation Rate Coefficients $J(O^1D)$ and $J(NO_2)$

Cirrus, observed to occur in the upper troposphere mainly in the tropics, attenuate solar radiation with subsequent effects on photodissociation processes concerning atmospheric ozone. Here, we present a theoretical study of the effects on $J(O^1D)$ and $J(NO_2)$ using observation-based cloud properties (Table 1). Due to the importance of multiple reflection between clouds at different altitudes, the case of cirrus with an underlying water cloud is also investigated.

It is found that in the tropics, cirrus clouds can significantly increase *J* values both above and below cirrus. Under overhead sun, a cirrus with a visible optical thickness 2 can increase the $J(O^1D)$ and $J(NO_2)$ below cirrus by 17 and 21% (Table 2 and Fig. 2), respectively. The values can be significantly increased, by a factor of 4 or more, when an underlying water cloud is present (Fig. 3). The observed stratospheric ozone depletion during the 1980s further enhances the increases throughout the atmosphere (Fig. 4). Sensitivity of the effects to cloud optical thickness, solar zenith angle and surface albedo is also examined.

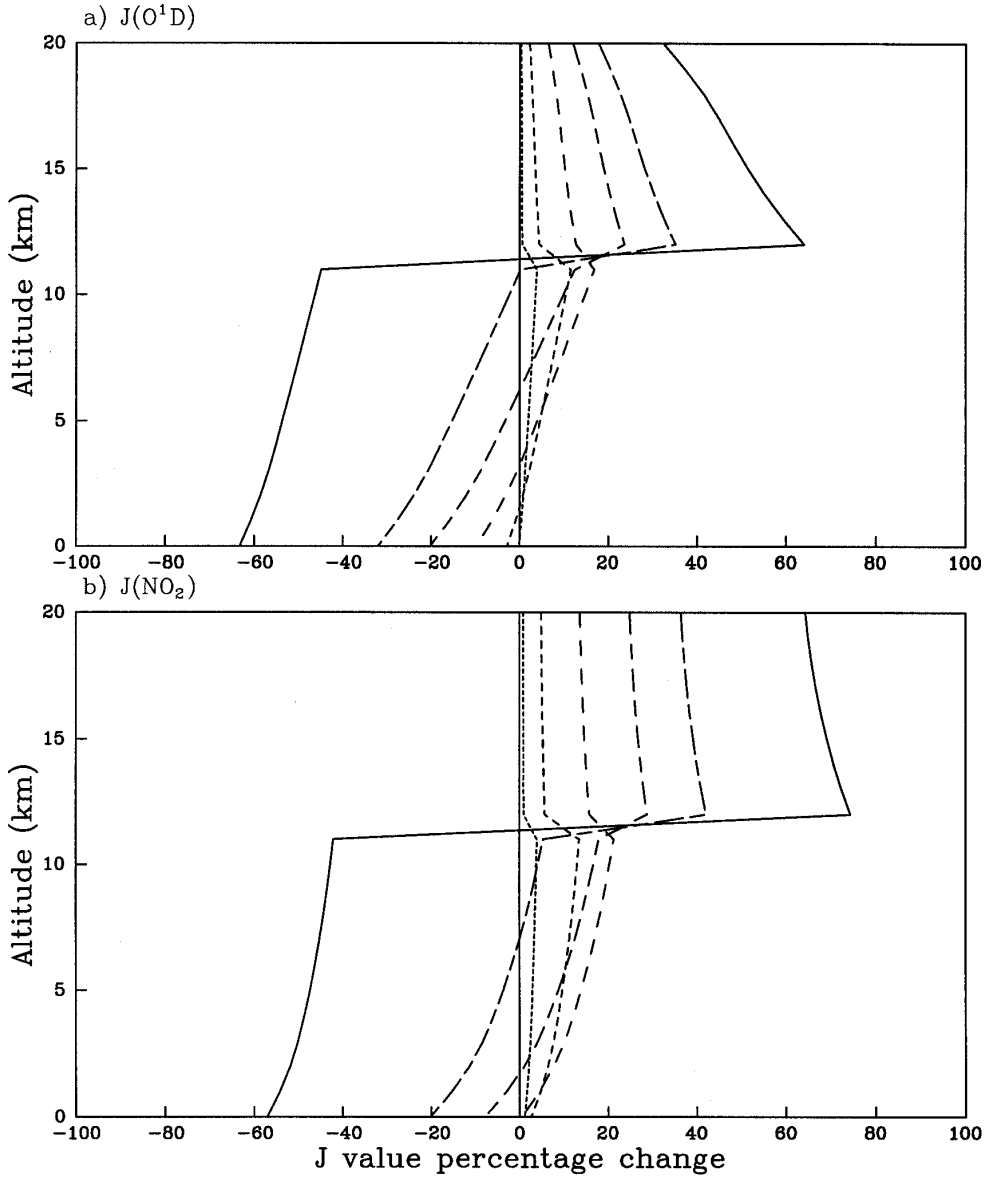

Fig. 2. Changes (versus clear sky; %) in (a) $J(O^1D)$ and (b) $J(NO_2)$ with six cirrus cloud optical depths under overhead sun in a standard tropical atmosphere. Shorter to longer dash lines followed by the solid line represent the six cirrus cloud optical depths in increasing order with values given in Table 1. The cloud is placed between 11 and 12 km and the surface albedo is 0.06.

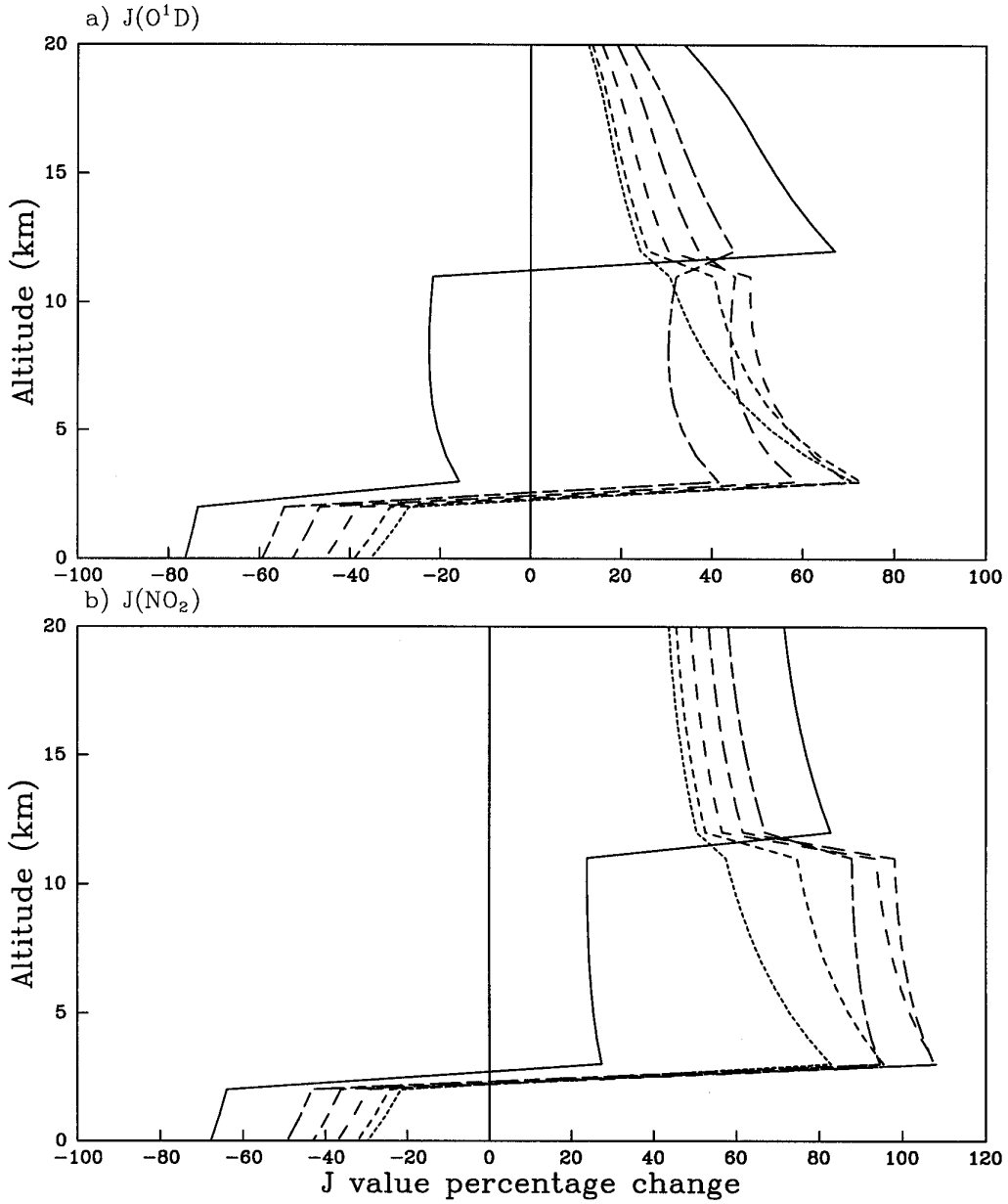

Fig. 3: The same as in Fig. 2 except that the cirrus (τ=2.43) is overlapped with a water cloud (τ=15) between 3 and 4 km.

Table 1: Physical and optical properties of tropical cirrus clouds based on the observation-derived ice water path (gm^{-2}) and effective radius (μm) by McFarquhar and Heymsfield (1996).

Parameter	I	II	III	IV	V	VI
ice water path	0.01022	1.02	10.2	102.2	204.3	1022.0
effective radius	16.2	40.9	43.5	55.9	67.6	105.5
optical depth	0.16	0.86	2.43	4.79	8.05	27.07
single scattering albedo	0.9997	0.9997	0.9997	0.9996	0.9993	0.9991
Asymmetry factor	0.78	0.78	0.79	0.79	0.80	0.82

Table 2: Changes (versus clear sky; %) in $J(O^1D)$ and $J(NO_2)$ above (below) the cirrus cloud without (Case I) and with (Case II) an underlying water cloud (τ=15) for overhead sun.

Case		Cirrus cloud optical depth					
		0.15	0.86	2.43	4.79	8.05	27.05
I	$J(O^1D)$	0.6 (3.9)	4.4 (12)	13 (17)	24 (12)	35 (0.2)	64 (-45)
	$J(NO_2)$	0.9 (3.9)	5.7 (13)	16 (21)	29 (18)	42 (5.3)	74 (-42)
II	$J(O^1D)$	24 (31)	26 (40)	30 (48)	37 (45)	45 (32)	67 (-22)
	$J(NO_2)$	50 (57)	52 (75)	57 (94)	62 (98)	67 (88)	83 (24)

3. The Impact on Radiative Forcing from Aircraft Emission

3.1 Aircraft emission scenarios

- **Reference Atmosphere**: The background atmosphere of year 2015 suggested by IPCC/IS92a. No aircraft emission
- **Perturb-I**: Reference + NASA 2015 subsonic aircraft emission
- **Perturb-II**: Reference + NASA 2015 subsonic and supersonic aircraft emission

3.2 Changes in ozone and water vapor

- The atmospheric gas species, including ozone and water vapor, and their changes due to aircraft emission are calculated using University of Oslo's 3-D chemical transport model.

- Changes in ozone and water vapor shown below correspond to:
-
  - Case A (Perturb-I minus Reference)--Effect of subsonic aircraft emission
  - Case B (Perturb-II minus Reference)--Effect of subsonic and supersonic aircraft emission—

3.3 Radiative forcing

- The solar and longwave radiative schemes of SUNYA-CCM3 are used to calculate the radiative fluxes using the global distribution of cloud, humidity and surface albedo from SUNYA-CCM3 AMIP simulation.
- For ozone distribution, we used the SUNYA ozone climatology (Wang et al., 1995) in the Reference Atmosphere while the percentage changes of ozone calculated from CTM are mapped onto the SUNYA ozone climatology for the perturbed atmosphere.
- For water vapor, we add directly the CTM calculated change of water vapor to the CCM3 simulated water vapor distribution for the perturbed atmosphere.
- Fixed dynamics treatment, which allows for the temperature changes in respond to changes in ozone and water vapor, is used to calculate the radiative forcing of the troposphere-surface climate system.

Table 3: Radiative forcing (Wm^{-2}) due to aircraft emission at year 2015. Values are for Case A (the effect of subsonic aircraft emission) while values in parentheses are for Case B (the combined effect of subsonic and supersonic aircraft emission).

	January		July	
	0-90°N	**0-90°S**	**0-90°N**	**0-90°S**
Total	0.027(0.052)	0.022(0.030)	0.063(0.075)	0.023(0.042)
Ozone	0.019(0.015)	0.020(0.023)	0.054(0.049)	0.015(0.015)

	15°**N-30°N**	20°**S-35°S**	**30°N-45°N**	0-15°**S**
Total	0.043(0.075)	0.035(0.051)	0.087(0.110)	0.036(0.055)
Ozone	0.034(0.030)	0.028(0.033)	0.077(0.071)	0.029(0.032)

4. The SUNYA AMIP-II Ozone Experiments

- Atmospheric ozone is a chemically important climate gas. Ultimately, an interactive climate-chemistry model is required to simulate ozone distribution. Most global climate models use climatological zonal mean ozone without considering its longitudinal and interannual variations. Therefore, in parallel to the interactive model development, an understanding of how the variability of ozone affects the simulated climate is warranted.

- To do this, the ozone data (Wang et al., 1995), which includes the spatial and temporal ozone variability, is incorporated into SUNYA-CCM3 to conduct AMIP-II experiments. We intend to investigate:

  - How longitudinal ozone variation affects the simulated thermal and dynamical structure as well as their implications on long-lived tracer transport; and
  - How interannual variation in total column ozone affects interannual climate variability.

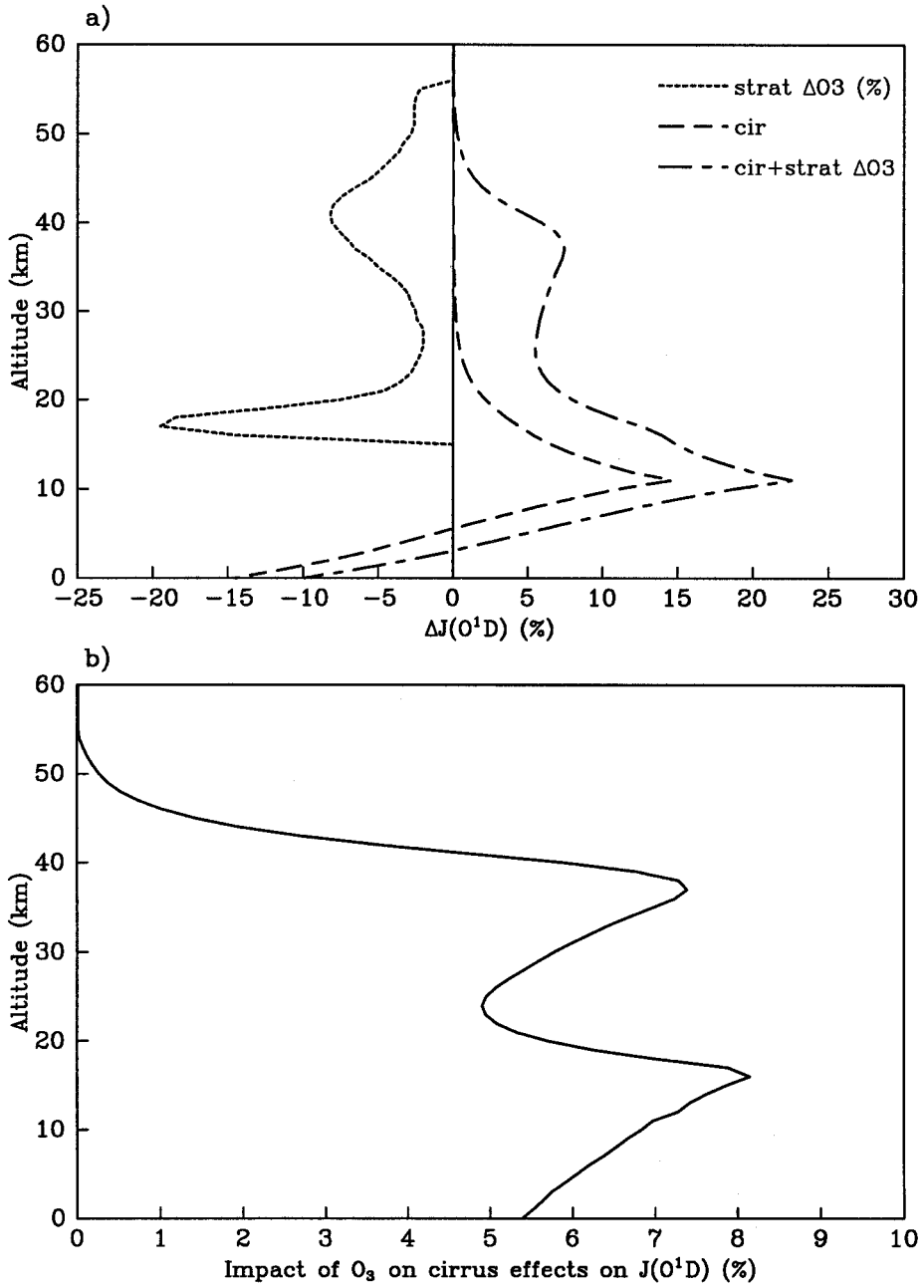

Fig. 4. (a) The observed stratospheric O_3 depletion during the 1980s at midlatitudes (dot), the J-value changes due to the cirrus cloud (τ=2.43; dash) and the J-value changes due to the combined ozone depletion and cirrus cloud (dot-dash); (b) The effect of ozone depletion on the changes of $J(O^1D)$ due to cirrus.

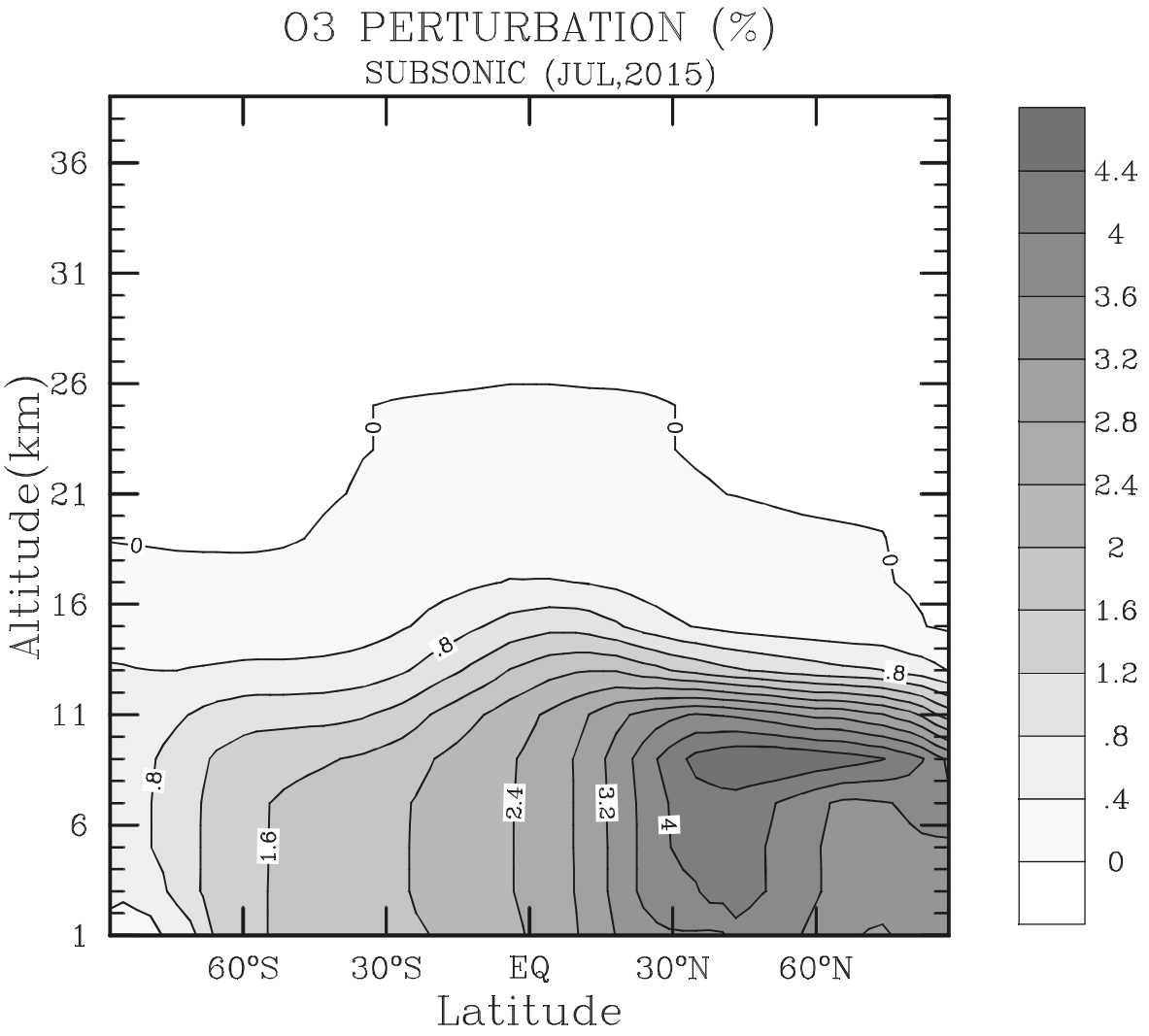

Fig 5A. Altitude-latitudinal distribution of ozone changes in July for Case A.

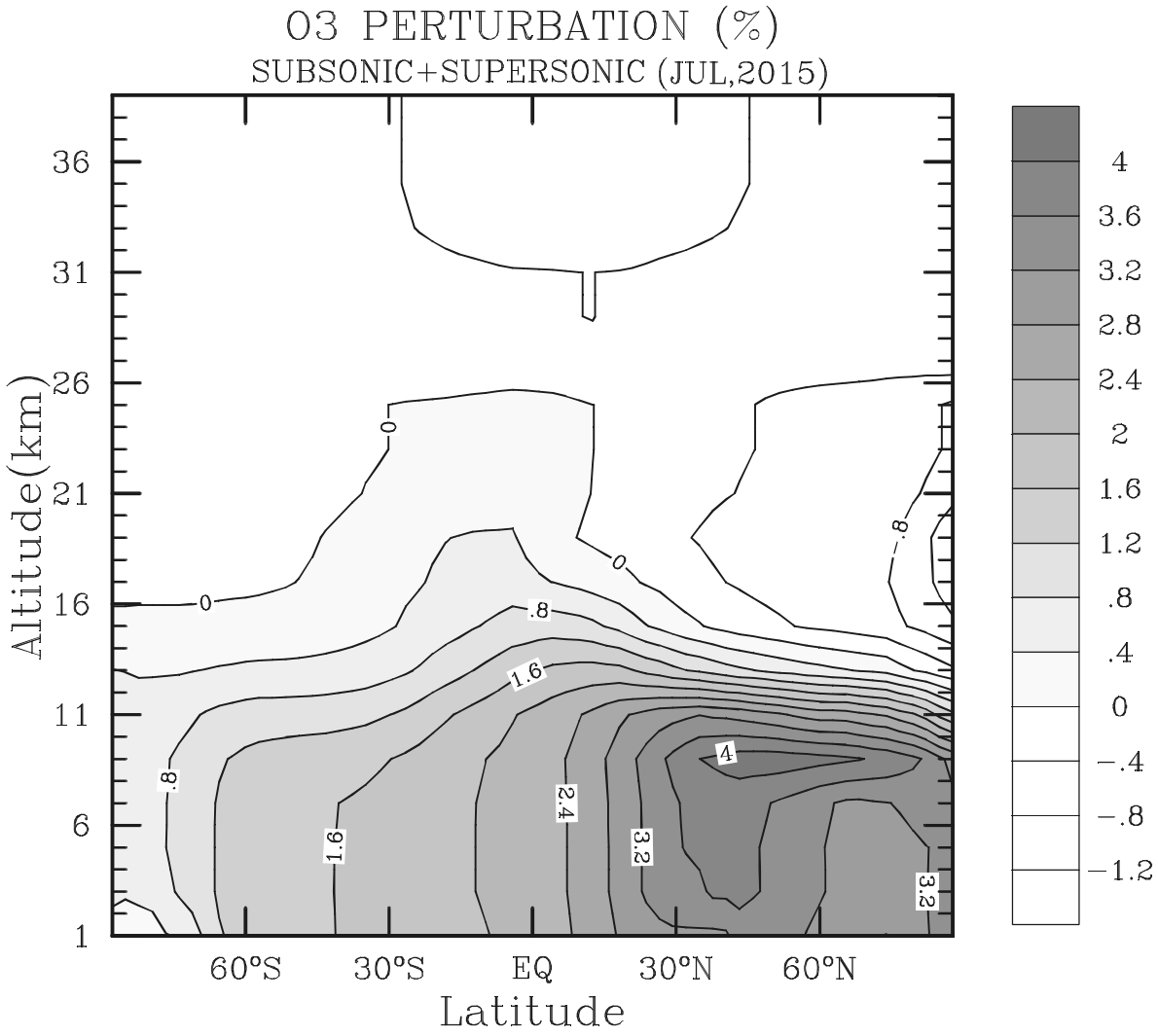

Fig 5B. Altitude-latitudinal distribution of ozone changes in July for Case B.

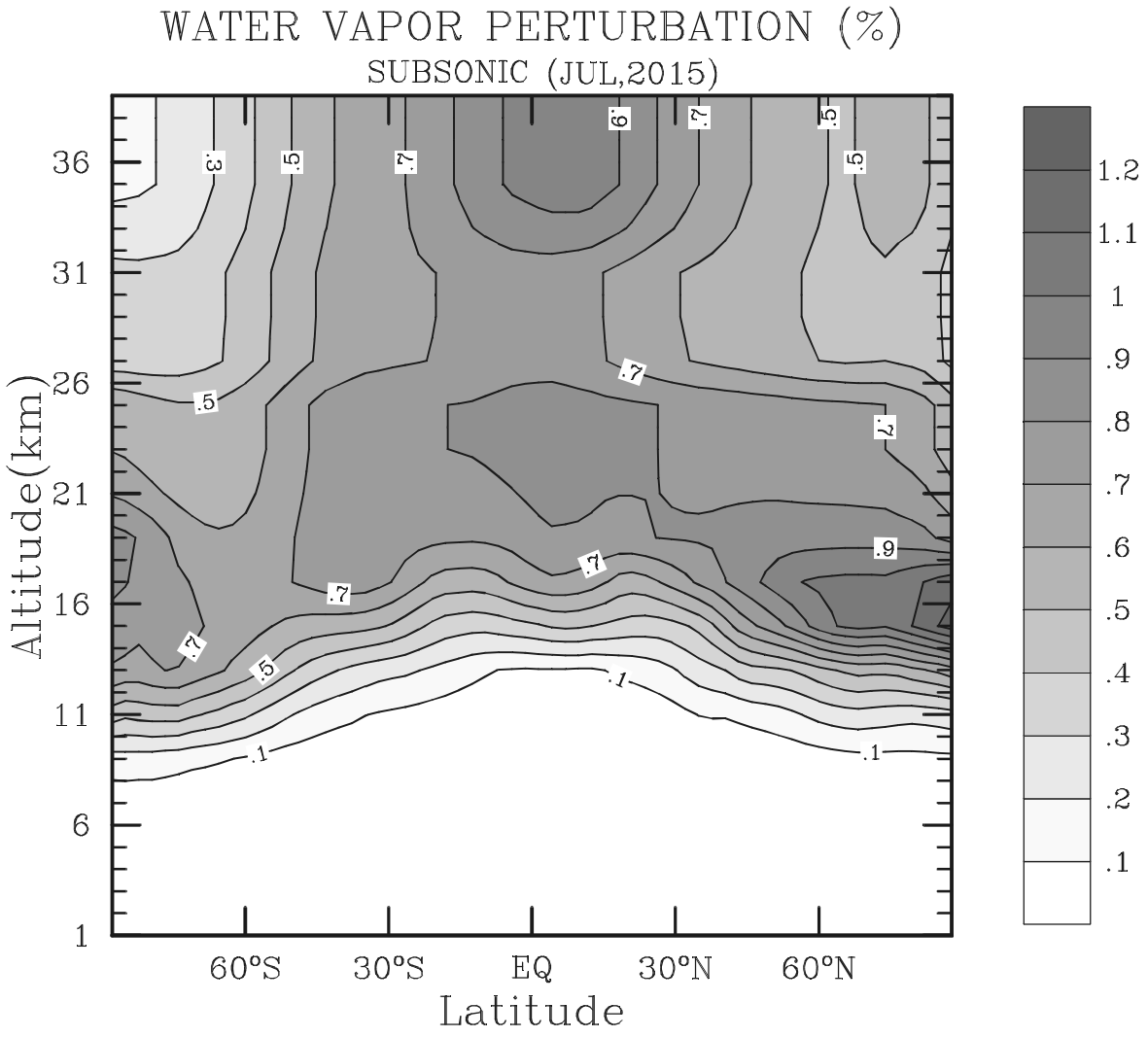

Fig 6A. Same as in Fig. 5 except for changes in water vapor.

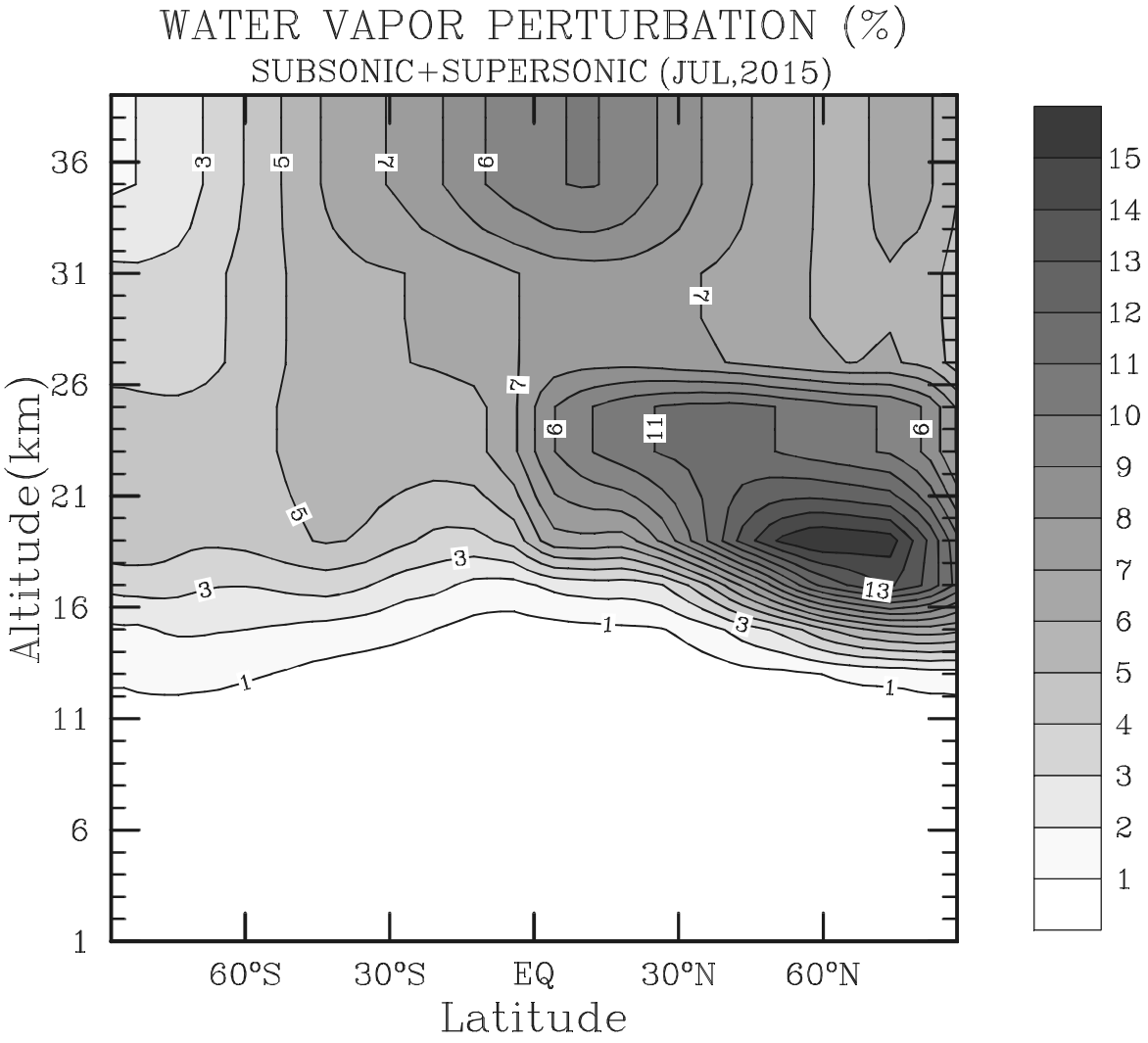

Fig 6B. Same as in Fig. 5 except for changes in water vapor.

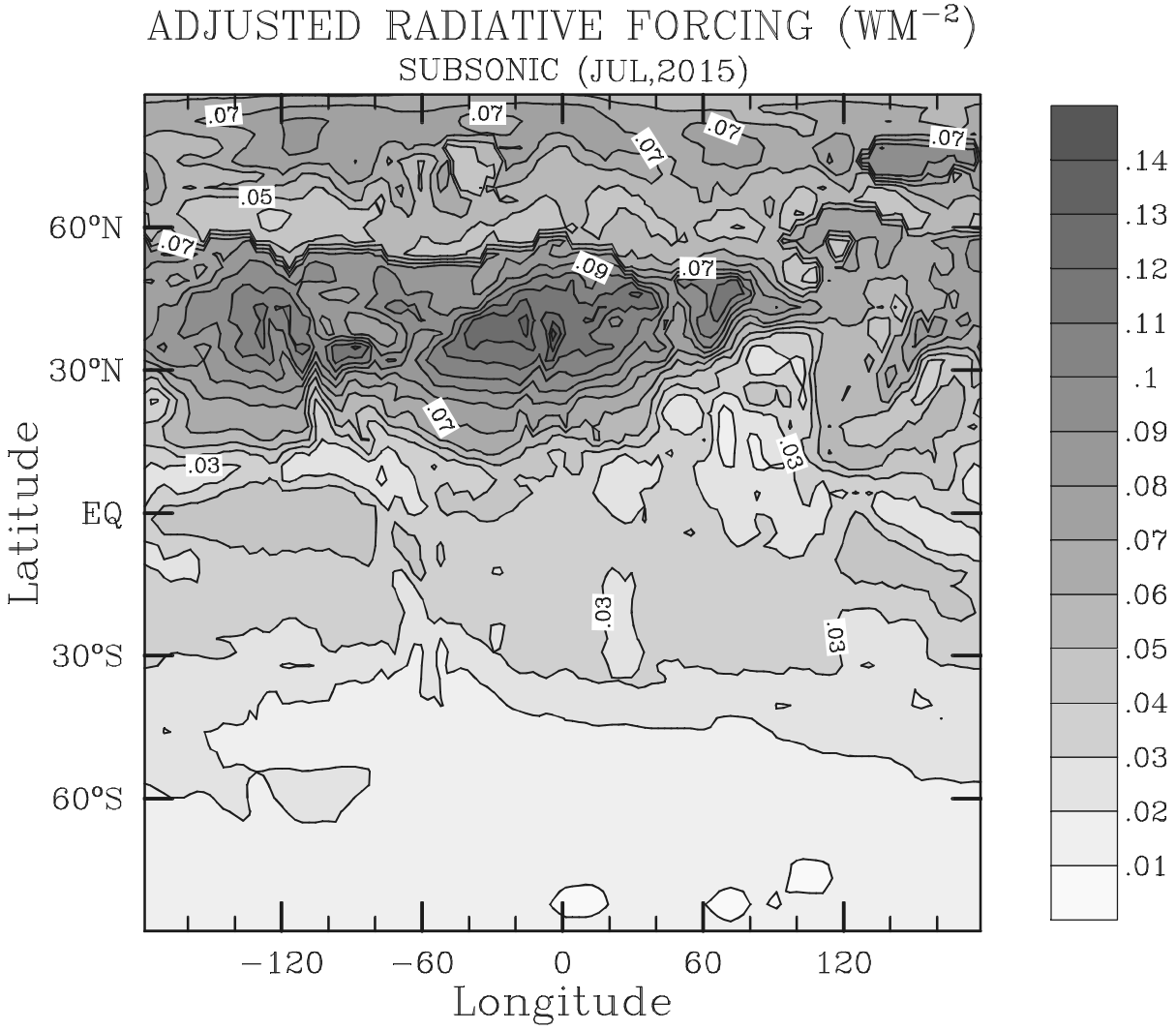

Fig. 7A. Latitude-longitudinal distribution of July radiative forcing for Case A.

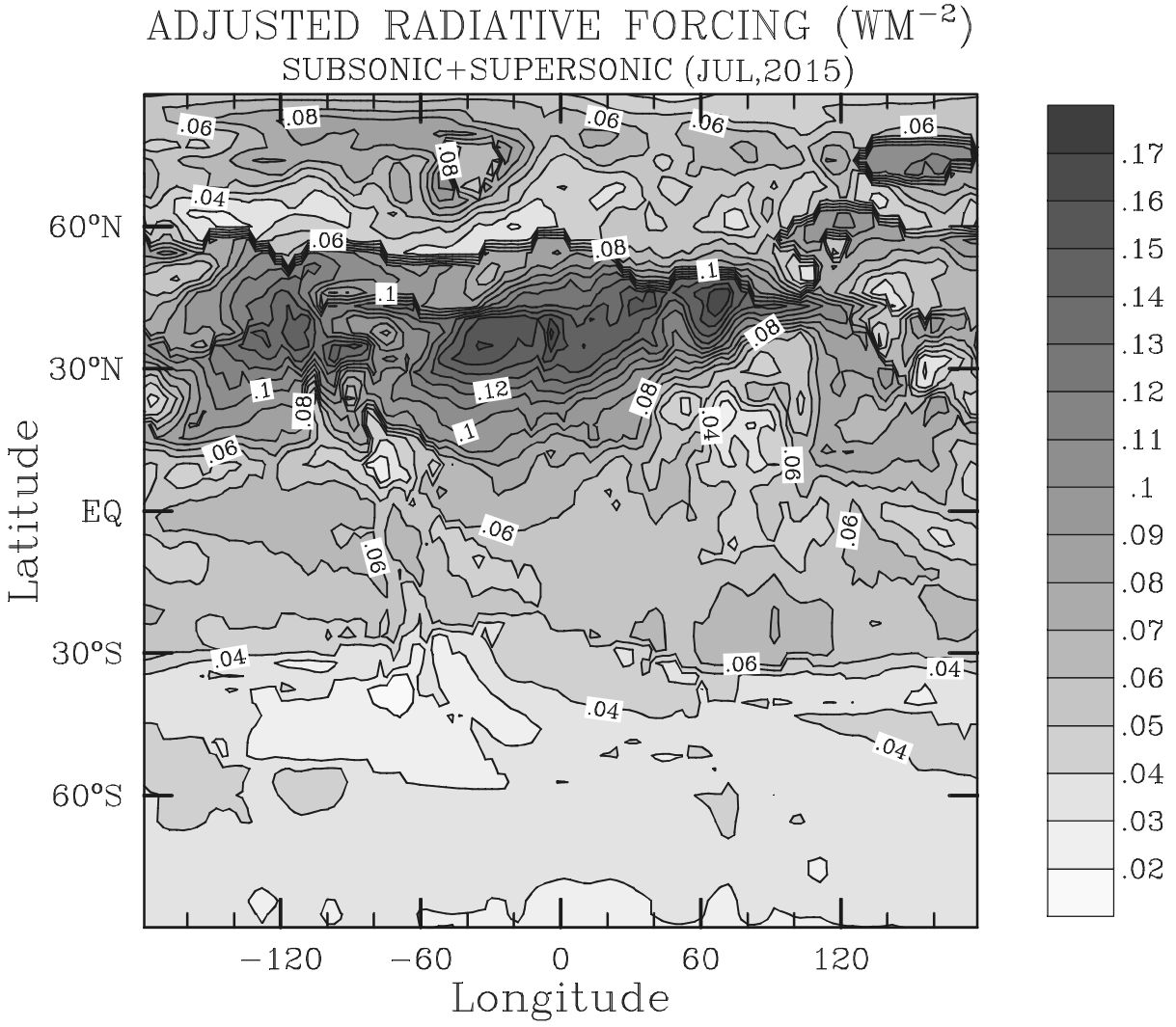

Fig. 7B. Latitude-longitudinal distribution of July radiative forcing for Case B.

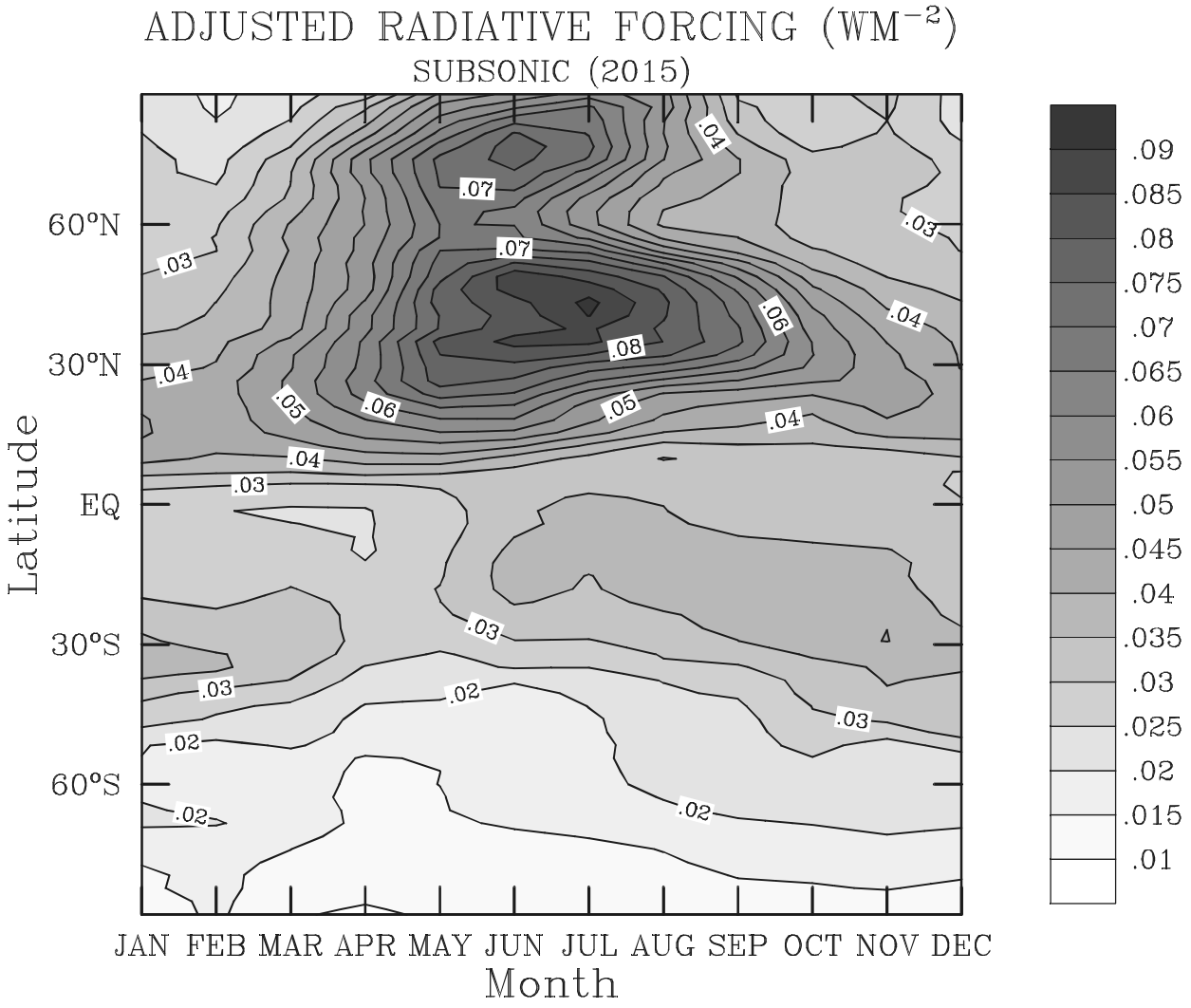

Fig. 8A. Month-latitudinal distribution of radiative forcing for Case A.

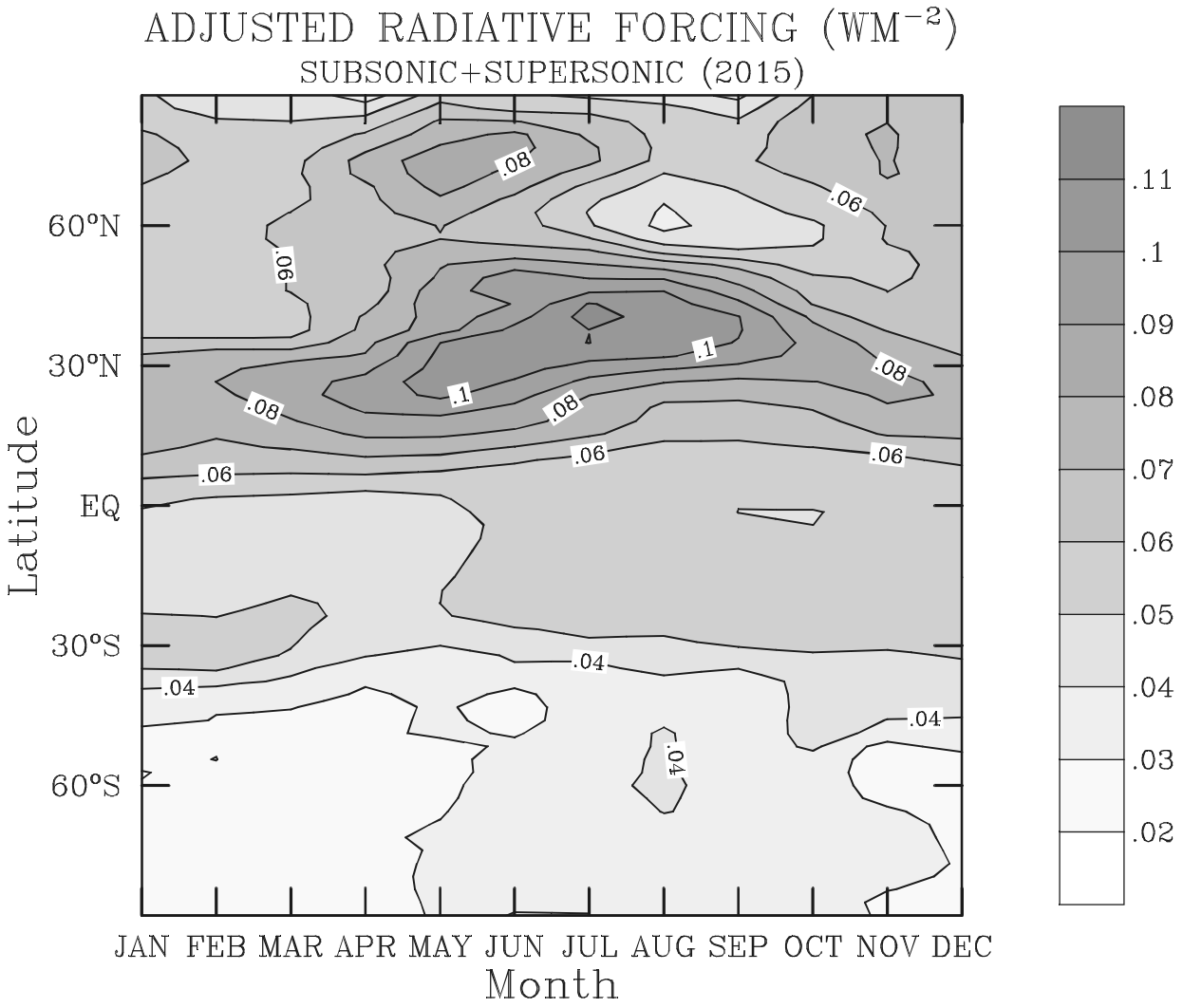

Fig. 8B. Month-latitudinal distribution of radiative forcing for Case B.

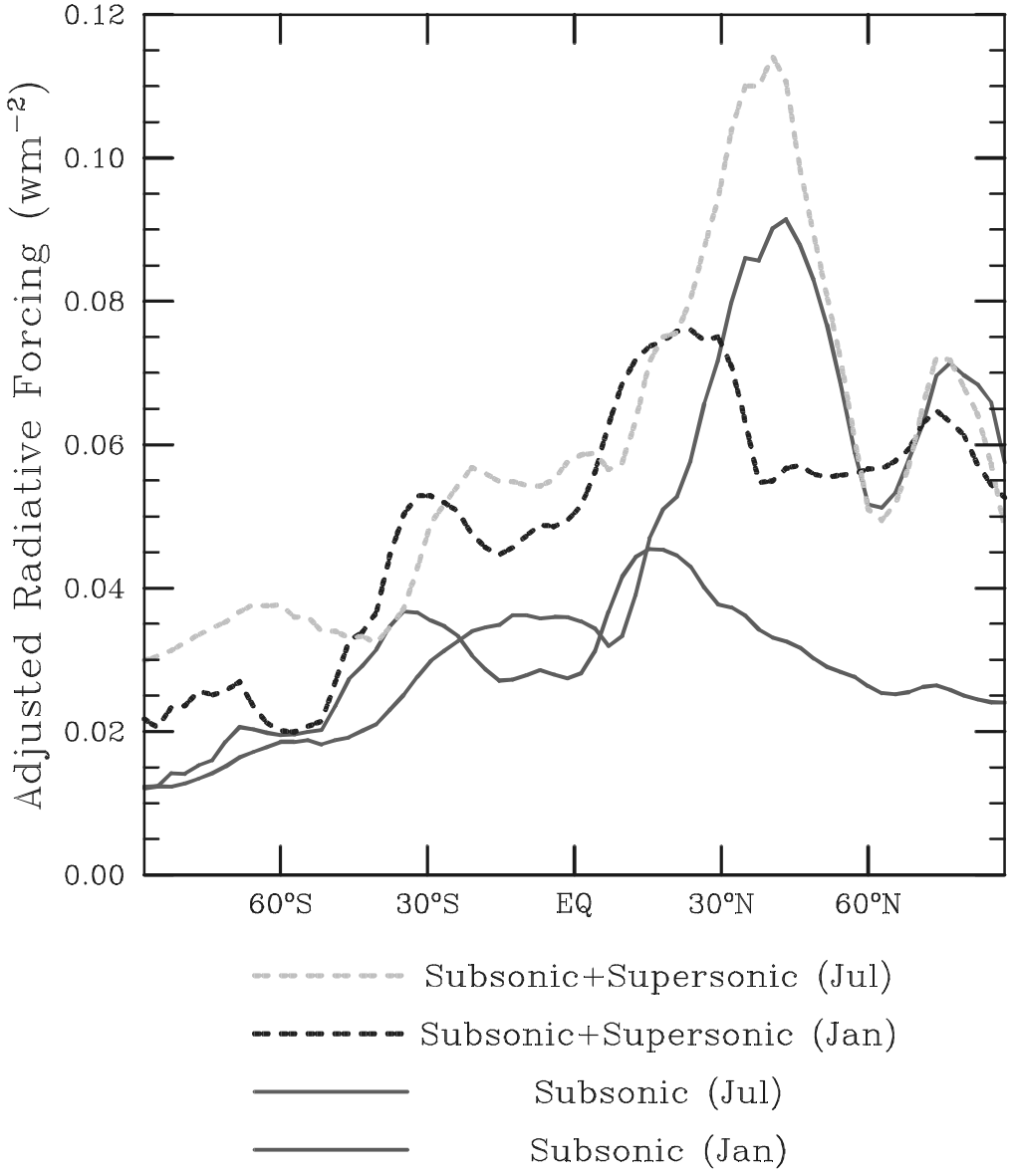

Fig. 9. Zonal mean distribution of radiative forcing for January and July of Cases A and B.